IEEE Access
Multidisciplinary | Rapid Review | Open Access Journal

Received December 26, 2018, accepted January 10, 2019, date of publication January 18, 2019, date of current version February 6, 2019.

Digital Object Identifier 10.1109/ACCESS.2019.2893230

220-320 GHz Hemispherical Lens Antennas Using Digital Light Processed Photopolymers

NONCHANUTT CHUDPOOTI[1], (Member, IEEE), NATTAPONG DUANGRIT[2], PRAYOOT AKKARAEKTHALIN[2], (Member, IEEE), IAN D. ROBERTSON[3], (Fellow, IEEE), AND NUTAPONG SOMJIT[3], (Member, IEEE)

[1]Department of Industrial Physics and Medical Instrumentation, Faculty of Applied Science, King Mongkut's University of Technology North Bangkok, Bangkok 10800, Thailand
[2]Department of Electrical and Computer Engineering, Faculty of Engineering, King Mongkut's University of Technology North Bangkok, Bangkok 10800, Thailand
[3]School of Electronic and Electrical Engineering, University of Leeds, Leeds LS2 9JT, U.K.

Corresponding author: Nonchanutt Chudpooti (nonchanutt.c@sci.kmutnb.ac.th)

This work was supported in part by the Thailand Research Fund through the TRF Senior Research Scholar Program under Grant RTA 6080008, in part by the Royal Golden Jubilee Ph.D. Program under Grant PHD/0056/2558, and in part by the Engineering and Physical Sciences Research Council under Grant EP/N010523/1 and Grant EP/N005686/1.

ABSTRACT This paper presents a 220–320-GHz hemispherical lens antenna fabricated using photopolymer-based additive manufacture and directly fed by the standard WR-3 rectangular waveguide without any additional waveguide extension. The microfabrication process is based on digital light processing rapid prototyping using the Monocure 3DR3582C resin-based photocurable polymer. This gives various key advantages, including ease of antenna fabrication, manufacturing speed, and cost-effectiveness due to its rapid fabrication capability. Even though the photopolymer is found to have a loss tangent of 0.034 at 320 GHz, the all-polymer lens antennas still achieve a fractional bandwidth of 37%, covering the whole 220–320-GHz WR-3 waveguide band with a measured gain of approximately 16 dBi at 0° over the whole band. A measured return loss of better than 14 dB is achieved from 220 to 320 GHz with a half-power beamwidth of approximately 12°, which is relatively constant over the whole WR-3 band.

INDEX TERMS Lens antenna, digital light processing, terahertz antennas.

I. INTRODUCTION

Terahertz (THz) technology attracts more and more attention from researchers and engineers from all over the world because of its important potential applications, such as high-resolution radars, imaging systems, sensing, security scanning, and high-speed communications [1]–[10]. Antennas are, of course, key components used in these applications. In recent years, many types of THz antenna have been reported, such as horn antennas, slotted waveguide antennas, reflector antennas, and dielectric lens antennas [11]–[28]. Among these, dielectric lens antennas are very attractive for many THz applications due to their simple structure, high gain, broadband characteristics, zero conductor losses and circular polarization [19]–[25].

Additive manufacturing rapid prototyping technology, also known as 3D printing technology, has also been playing an important role in state-of-the-art 3D fabrication processes because of its fast prototyping capability and low manufacturing costs, with various dielectric and conductor materials available for use in 3D printing processes. Among the various additive manufacturing techniques, fused deposition modeling (FDM), digital light processing (DLP) and polymer jetting (PolyJet) are most often used for fabricating millimeter-wave and THz components such as antennas [29]–[31], waveguides [32], [33], and THz sensors [34], [35]. However, due to its capability in fabricating high-resolution 3D structures and various choices of printing materials, the DLP technique is often preferred to FDM and PolyJet fabrication.

In this paper, all-photopolymer hemispherical lens antennas operating from 220 to 320 GHz are reported, fabricated with a DLP additive manufacturing process using Monocure-3DR3582C resin-based photocurable polymer. A cavity fabricated at the base of the lens structure is used to match the impedances between the aperture of the WR-3 rectangular feed and the hemispheric lens antennas, optimizing the reflection coefficient (S_{11}) of the antennas to better than -10dB and maximizing the operational fractional

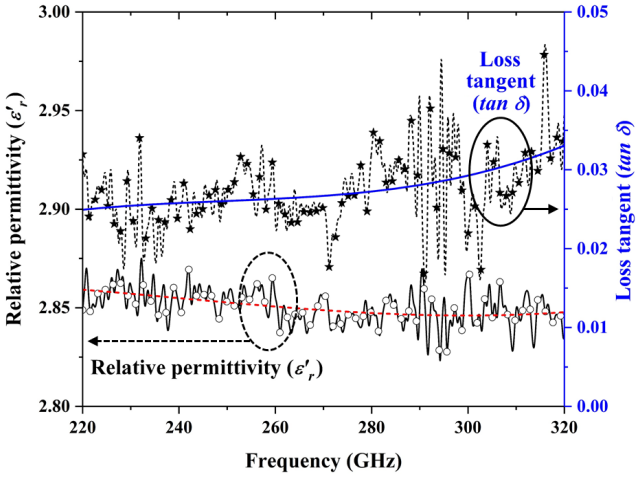

FIGURE 1. The measured dielectric constant and loss tangent of Monocure 3DR3582C photopolymer material from 220–320 GHz, determined using the Keysight Technologies 85071E material characterization suite. The red and blue traces are third-order polynomial regression curve fits.

bandwidth to cover the whole of the WR-3 band. The form factor of the hemispheric lens antennas was optimized as a balanced compromise between the antenna realized gain and photopolymer material losses of Monocure 3DR3582C. However, the realized gain of the lens design in this work can be easily enhanced by using lower loss photopolymers as alternatives to Monocure 3DR3582C. This work introduces several advantages e.g. ease of antenna design and fabrication based on all-photopolymer 3D structures as well as fabrication cost effectiveness and prototyping speed. Moreover, the hemispherical lens antennas can be precisely mounted directly at the waveguide ports of the VNA extender without any additional waveguide section or waveguide transition.

II. LENS ANTENNA DESIGN AND FABRICATOIN

A. PHOTOPOLYMER CHARACTERIZATION

Monocure 3DR3582C rapid-photocurable resin-based polymer [36] is used to fabricate the hemispherical lens antennas due to its low cost and commercial availability. The Keysight Technologies free-space material characterization suite 85071E [37] was used with a PNA-X vector network analyzer (VNA) and OML frequency extenders to measure the dielectric properties of the Monocure photopolymer in the WR-3 band. Figure 1 plots the dielectric constant and loss tangent of the Monocure 3DR3582C photopolymer from 220 – 320 GHz. Over the whole WR-3 band, the third-order polynomial regression fitted dielectric constant changes slightly from 2.86 to 2.85 while the curve-fitted loss tangent increases from 0.025 to 0.033 over the 220 to 320 GHz range. From the free-space measurement results, the dielectric constant variation from 2.85 and 2.86 does not pose a problem for designing a broad range of millimeter-wave and THz components as well as various THz antennas. However, the loss tangent is relatively high compared to conventional but costly dielectric materials such as high-resistivity silicon or

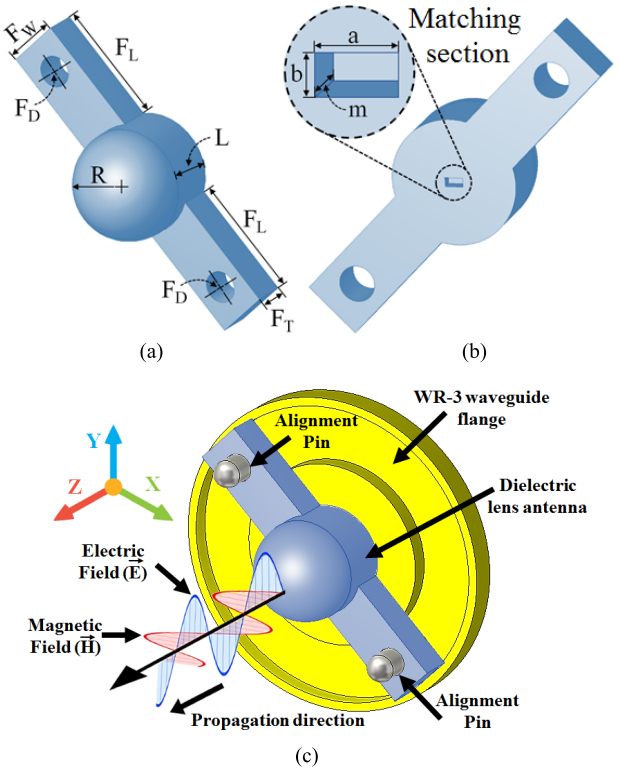

FIGURE 2. 3D perspective views of the 220-330 GHz all-photopolymer lens antenna: (a) front view, (b) back view and (c) the hemispheric lens antenna mounted on the WR-3 rectangular waveguide flange of the network analyzer frequency extender.

GaAs substrates. On the other hand, the price of the photopolymer is much lower than those of conventional dielectric substrates and it is easy to form 3D microstructures with much lower fabrication costs, making the photopolymer very attractive for many millimeter-wave and THz applications.

B. LENS ANTENNA DESIGN

Lens antennas are very attractive for many applications in millimeter-wave and THz systems due to their high gain, compared to most planar antennas, and ease of design and fabrication compared to other high-gain antenna elements such as horn and parabolic antennas. Hemispherical lenses are the simplest 3D structures for lens antenna designs while still offering various advantages such as circular polarization properties and broadband characteristics. In this work, the 3D full-wave EM simulation package CST Studio Suite was used to design the 220-320 GHz hemispheric lens antennas based on Monocure 3DR3582C photopolymer. The values of all necessary parameters are shown in Table 1. Fig. 2(a) and (b) depict the front and back side of the hemispheric lens, respectively, with the mechanical and electrical design parameters labeled.

The radius of the hemispherical antenna, R, determines the gain of the antenna while the extension length of the antenna, L, is optimizable to reduce the overall side lobe characteristics of the antenna radiation pattern [24]. F_W and

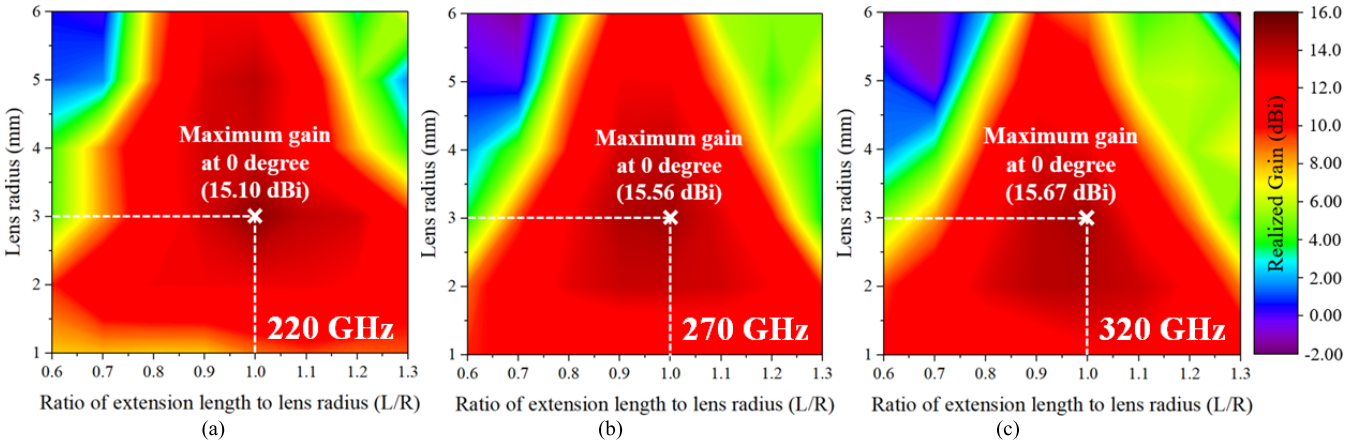

FIGURE 3. Modeled gain of the all-polymer lens antenna plotted as a function of lens radius (R) and ratio between the extension length and lens radius (L/R). The contour plots show the realized gain at 0° (boresight) for three chosen frequencies, (a) lower frequency of 220 GHz, (b) mid-band frequency of 270 GHz, and (c) upper frequency of 320 GHz. The maximum values of the realized gain at 220 GHz, 270 GHz and 320 GHz, are 15.10 dBi, 15.56 dBi, and 15.67 dBi, respectively. At the maximum points, the value of lens radius is 3 mm and ratio of extension length to lens radius (L/R) is 1.0 for all selected frequencies.

TABLE 1. Dielectric lens antenna geometry.

Parameter	Description	Optimum value (mm)
R	Lens radius	3.00
L	Extension length	3.00
F_W	Fixture width	3.00
F_D	Fixture diameter	1.70
F_L	Fixture length	6.40
F_T	Fixture thickness	2.00
a	Matching length	0.86
b	Matching width	0.43
m	Matching depth	0.20

F_L are the width and length of the antenna mechanical fixtures, respectively, with screw hole diameters of F_D, which are used to directly mount the antennas to the WR-3 rectangular waveguide flanges, providing mechanical stability during the free-space antenna measurements. The fixture thickness, F_T, was carefully chosen to minimize any electromagnetic (EM) effects of the antennas, e.g. degradation of the radiation characteristics and return loss, while still maintaining stable mechanical properties between the waveguide feed and the lens. In order to maximize the EM power coupling from the WR-3 feed to the lens antenna, an impedance matching section using a cavity with dimensions of a, b and m, as shown in Fig. 2(b), is introduced at the base of the antennas. Fig. 2(c) illustrates the 3D structure of the hemispheric lens antennas mounted with WR-3 rectangular waveguide feed, along with the orientation of the EM fields and the direction of radiation.

The optimum ratio between the extension length and lens radius (L/R) was simulated and obtained by using the 3D EM simulation tool CST Studio Suite. Parametric sweep simulation was used to vary the lens radius from 1 mm to 6 mm with a step of 1 mm and the ratio of the extension length to lens radius (L/R) from 0.6 to 1.3 with a step of 0.05. From the parametric sweep simulations, the realized gain at 0° for three frequencies representing lower, mid-band and upper frequencies of the lens antennas, which are at 220, 270 and 320 GHz, respectively, were recorded. Three contours, as a function of lens radius R and ratio of the extension length to lens radius L/R of the three selected frequencies, are plotted in Fig. 3, and these were used to determine the maximum values of realized gain. From the simulations, the effect of the dielectric properties, i.e., dielectric constant and loss tangent, were carefully considered to investigate their effect on the lens antenna performance. In Fig. 3, the maximum realized gain at 0° of the lens antennas for all three frequencies is achievable approximately at the same values of lens radius ($R = 3$ mm) and ratio between the extension length and lens radius ($L/R = 1.0$). For the lens radius longer than 3 mm ($R > 3$ mm), the contour plots indicate decreasing realized gains for all three selected frequencies, caused by the EM power loss in the dielectric material. Thus, the loss tangent of material plays an important role in the design optimization and should be considered early in the mm-wave and THz lens antenna design process.

C. LENS ANTENNA MATCHING

For the all-polymer lens antenna without impedance matching, the best achievable reflection coefficient, S_{11}, is in the range of only −8 to −10 dB for the WR-3 band frequencies from 220 to 320 GHz. To minimize the signal reflection, an air-pocket cavity, which was introduced and published in [24] and [25], was implemented at the feed point of the hemispherical lens antenna to decrease the impedance mismatch level between the aperture of the open-ended waveguide feed and the lens. The air-pocket matching introduces various advantages e.g. less sensitivity of the impedance of the lens antenna to small distance variation between feed point and lens antenna. Fig. 4 shows the simulation results of

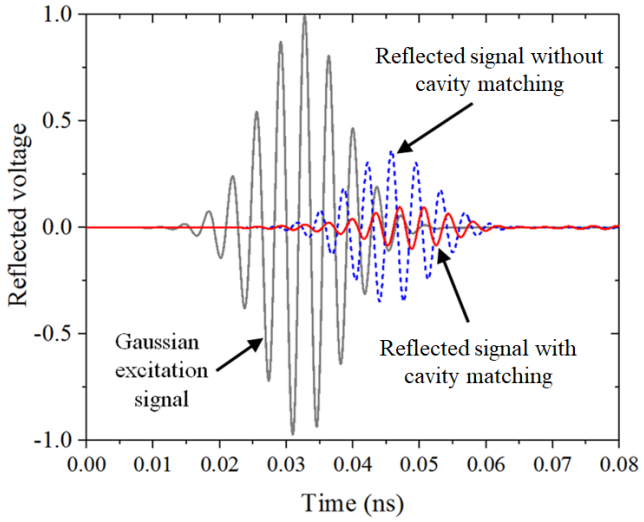

FIGURE 4. Comparisons of simulation results of signal reflections at the feed point in the time domain for the hemispherical lens antenna with and without cavity impedance matching.

the time-domain signal reflections at the antenna feed point between with and without the impedance matching section using CST Studio Suite. From Fig. 4, an incident Gaussian EM excitation signal was generated at the aperture of the waveguide feed. At the interface boundary between the aperture of the open-ended waveguide and air-pocket, the reflected signal voltages with and without the cavity matching are 0.12V (−18.41dB) and 0.36V (−8.87dB), respectively, as compared to the Gaussian input voltage of 1V (0 dB). The dimensions of the cavity were carefully determined by considering the achievable fabrication resolution of the 3D printer, ANYCUBIC Photon [38], used in this work. From Fig. 2 (b), the cross-section of the cavity matching section is fixed to $a = 0.8636$mm and $b = 0.4318$mm due to the inside dimensions of the standard WR-3 waveguide used to measure the lens antennas. The matching depth, m, was investigated by parametric sweep with the range from 0.1–0.4 mm with a step of 0.1mm. Figs. 5 (a) and (b) show the simulation results of the reflection coefficients and realized gain, as functions of matching section depth, at the radiation direction at 0°, respectively. From the simulation results, a matching section depth of 0.2 mm is chosen as the best compromise between the reflection coefficient and realized gain of the antenna, considering the additive manufacturing fabrication resolution as a design factor.

D. LENS ANTENNA FABRICATION

The hemispherical lens antenna was fabricated by using an ANYCUBIC Photon 3D printer [38] featuring DLP manufacturing technique with an integrated UV light source operating at a wavelength of 405 nm. The Monocure 3D rapid clear photopolymer [36], which is sensitive to a very wide range of wavelengths (225 to 420nm) was selected as the photopolymeric material for fabricating the lens antenna. The 3D models of the all-polymer lens antennas were

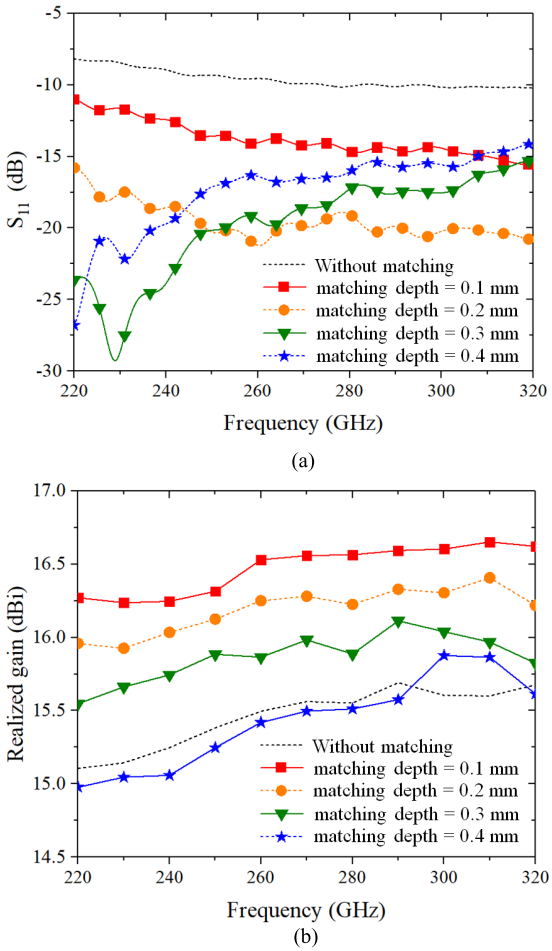

FIGURE 5. Simulated parametric study of the matching section depth, m, for (a) reflection coefficients (S_{11}) and (b) realized gain of antenna at 0°.

TABLE 2. The dimensions of dielectric lens antenna between design and fabrication.

Parameters	Design values (mm)	Actual values (mm)	Parameters	Design values (mm)	Actual values (mm)
R	3.00	2.96	F_T	2.00	1.98
L	3.00	2.98	a	0.86	0.87
F_W	3.00	3.00	b	0.43	0.44
F_D	1.70	1.72	m	0.20	0.22
F_L	6.40	6.39			

exported from the EM simulation package using the STL file format. The STL code was then converted into the machine language (G-code) by using the ANYCUBIC Photo slicer software with the layer thickness set to 0.025 mm, normal exposure time of 9.7 seconds, off time of 6.5 seconds, bottom exposure time of 65.5 seconds, and bottom layer curing of 8 layers. The total printing time of the all-polymer lens antenna including UV-curing and drying processes was 75 minutes with a possibility of batch processing for mass production. However, during the fabrication process,

TABLE 3. Key factor comparison of measurement of this work and other works.

Key Factor	[15]	[16]	[18]	[24]	[27]	*This work*
Operating frequency (GHz)	215 – 240	160 – 260	320 – 380	230 – 310	530 – 590	***220 – 320***
Antenna structure	Hemisphere dielectric lens	Square diffractive micro-lens array	Square grooved-dielectric lens	Hemisphere dielectric lens	Hemisphere silicon lens	***Hemisphere dielectric lens***
Antenna material	ABS	Nb_5N_6 microbolometer	Teflon	Rexolite	Silicon	***Monocure 3DR3582C***
Antenna design complexity	Low	High	High	Low	High	***Low***
Fabrication process	3D printing	Microfabrication	N/A	CNC milling	Photolithography and deep reactive etching	***3D printing***
Fabrication complexity	Low	High	High	Moderate	High	***Low***
Maximum antenna gain (dBi)	18	N/A	26.1	30	~23	***16.09***
Fractional bandwidth (%)	~11	47.62	17.14	30	10.71	***37***

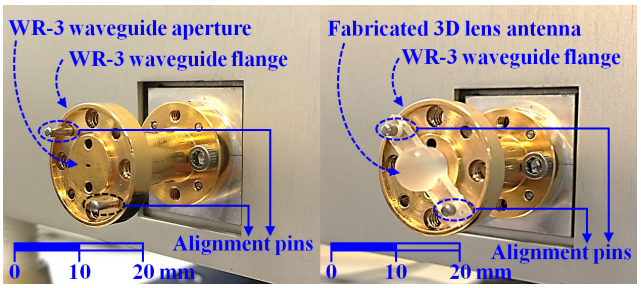

(a) (b)

FIGURE 6. (a) WR-3 waveguide flange without lens antenna (open-ended waveguide), (b) fabricated all-photopolymer lens antenna prototype mounted on the WR-3 waveguide flange.

the sacrificial raft and support patterns were manufactured to increase the mechanical stability of the lens antenna structures. The sacrificial patterns were afterward removed from the lens antennas at the final stage and have a small effect on the accuracy of the antenna fabrication. Table 2 lists the actual dimensions of the antennas measured by using an optical microscope compared to the design values.

III. MEASUREMENT RESULTS

To measure the reflection coefficient and radiation pattern of the all-photopolymer lens antenna, a Keysight Technologies PNA-X N5242 VNA with two OML WR-3 frequency extender heads was used with Line-Reflect-Line (LRL) calibration to measure the lens antennas from 220-320 GHz. A laser alignment system generally used in terahertz measurements was employed to accurately control the positioning and rotation of the antenna before and during the antenna measurement. Fig. 6 (a) shows the bare WR-3 waveguide extender port before attaching the all-photopolymer lens antenna while Fig. 6 (b) shows the lens antenna prototype attached to the WR-3 waveguide flange. The measured and simulated reflection coefficient, S_{11}, and realized gain at 0° for the whole WR-3 band from 220-320 GHz are plotted in Fig. 7.

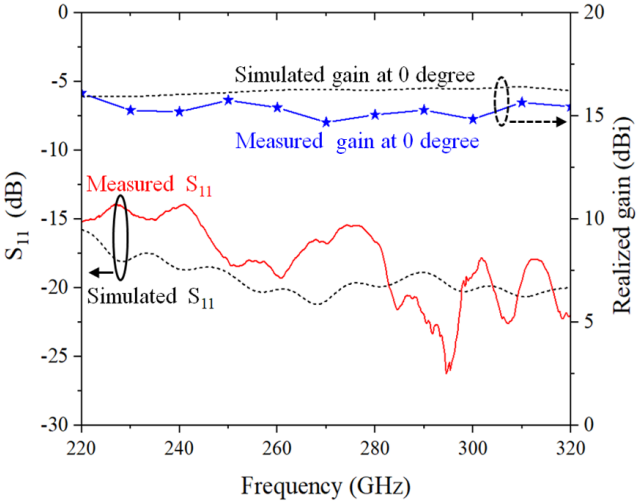

FIGURE 7. Comparison of simulated and measured reflection coefficient (S_{11}) and realized gain at 0 degree for the whole WR-3 band (220-320 GHz).

From the measurement results, it is shown that the antenna design in this work achieves the reflection coefficient well below 14 dB and relatively constant maximum antenna gain of approximately 16 dBi over the whole WR-3 band, with a calculated fractional bandwidth of 37%.

The radiation pattern of the all-polymer lens antenna at different frequencies was measured and compared to the radiation pattern of the open-ended WR-3 waveguide. A WR-3 horn antenna with nominal gain of 26 dBi and half-power beamwidth (HPBW) of 10° was used as the reference antenna for the free-space measurement. The Keysight VNA with extender heads was used to measure the radiation characteristics of the all-polymer lens antennas with the laser alignment system to control the positioning and rotation of the antenna during the radiation pattern measurement. The separation between the antenna-under-test (AUT) and reference antenna was set to 9 mm, which is well beyond

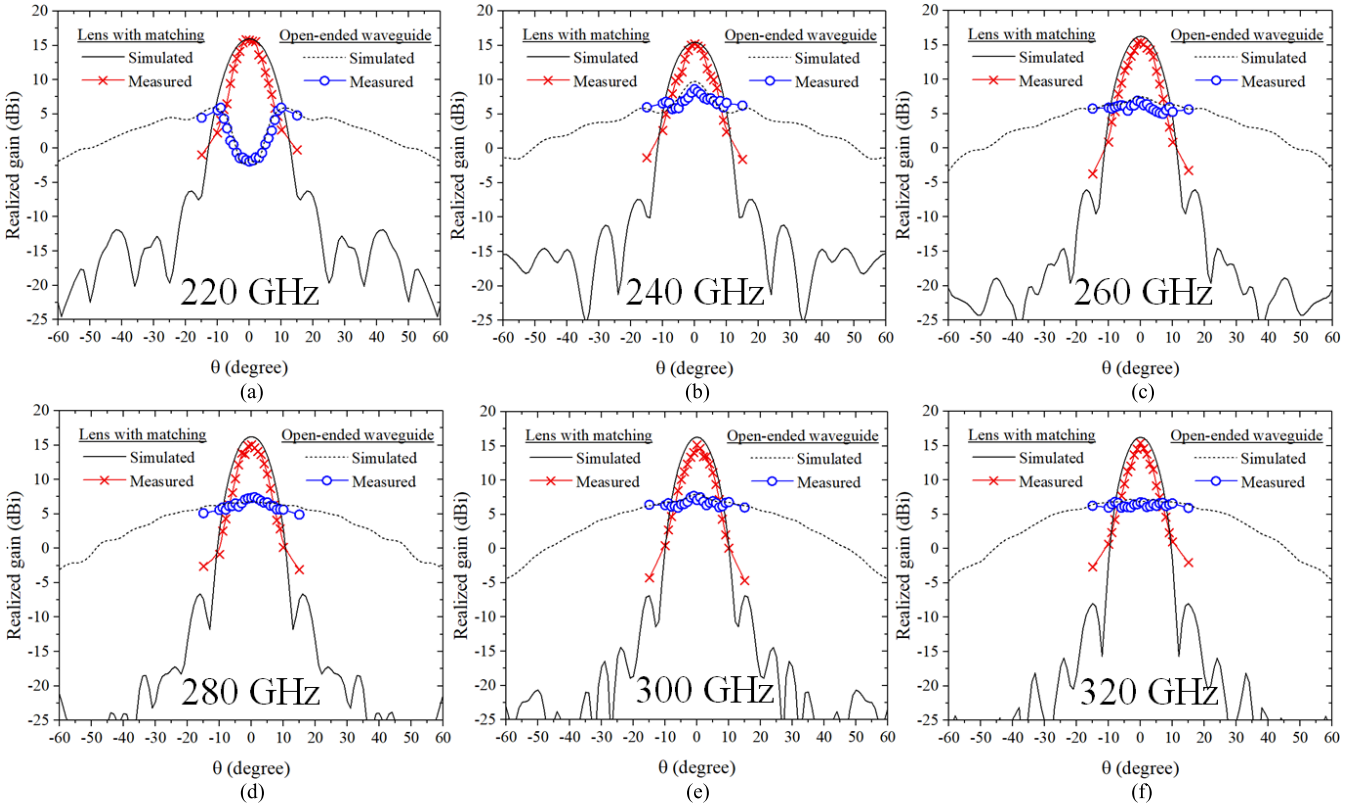

FIGURE 8. Comparison of simulated and measured radiation pattern of open-ended waveguide and proposed lens antenna with matching for (a) 220 GHz, (b) 240 GHz, (c) 260 GHz, (d) 280 GHz, (e) 300 GHz and (f) 320 GHz. The AUT was manually rotated from −15 degree to +15 degree with a step of 1 degree, with the desired distance and measurement angles checked using a laser alignment system.

the simulated far-field distance at the highest measurement frequency of 320 GHz. The AUT was manually rotated and precisely placed at the desired distances and at measurement angles from −15° to +15° with a step of 1° by using the laser alignment system. Fig. 8 (a)-(f) plots the radiation patterns at 220, 240, 260, 280, 300 and 320 GHz, respectively. From the measurement results, the HPBW of the all-polymer lens is approximately 12° with relatively constant maximum gain of 16.09dBi. The antenna design in this work compromises the gain and antenna form factor with the material loss of the photopolymer selected. To enhance the maximum realized gain, lower-loss materials are required such as high-resistivity silicon or GaAs but the material costs are usually high compared to the photo-curable polymers and 3D manufacturing is much more complicated. Moreover, the additive manufacturing fabrication process is much less complex for DLP technique compared to many conventional precision fabrications, e.g. cleanroom based, while mass production is still possible at very low fabrication cost. Table 3 compares figure-of-merits between the all-photopolymer lens antenna reported here and other state-of-the-art lens structures [15]–[16], [18], [24], [27] published to date.

IV. CONCLUSIONS

A 3D-printed all-photopolymer lens antenna operating over the full WR-3 waveguide band has been demonstrated. The antenna was fabricated by using a DLP additive manufacturing technique. The dielectric properties of the Monocure commercial photopolymer resin chosen for the antenna design have been precisely characterized by using a free space materials measurement system. The measured maximum gain of the all-polymer antenna is 16.09 dBi and a fractional bandwidth of 37% is achieved.

REFERENCES

[1] K. B. Cooper *et al.*, "A high-resolution imaging radar at 580 GHz," *IEEE Microw. Wireless Compon. Lett.*, vol. 18, no. 1, pp. 64–66, Jan. 2008.

[2] K. Ahi, "Mathematical modeling of THz point spread function and simulation of THz imaging systems," *IEEE Trans. THz Sci. Technol.*, vol. 7, no. 6, pp. 747–754, Nov. 2017.

[3] S. Sung *et al.*, "THz imaging system for *in vivo* human cornea," *IEEE Trans. THz Sci. Technol.*, vol. 8, no. 1, pp. 27–37, Jan. 2018.

[4] F. C. D. Lucia, D. T. Petkie, and H. O. Everitt, "A double resonance approach to submillimeter/terahertz remote sensing at atmospheric pressure," *IEEE J. Quantum Electron.*, vol. 45, no. 2, pp. 163–170, Feb. 2009.

[5] R. Dickie, R. Cahill, V. Fusco, H. S. Gamble, and N. Mitchell, "THz frequency selective surface filters for earth observation remote sensing instruments," *IEEE Trans. THz Sci. Technol.*, vol. 1, no. 2, pp. 450–461, Nov. 2011.

[6] R. Knipper *et al.*, "THz absorption in fabric and its impact on body scanning for security application," *IEEE Trans. THz Sci. Technol.*, vol. 5, no. 6, pp. 999–1004, Nov. 2015.

[7] R. Appleby and H. B. Wallace, "Standoff detection of weapons and contraband in the 100 GHz to 1 THz region," *IEEE Trans. Antennas Propag.*, vol. 55, no. 11, pp. 2944–2956, Nov. 2007.

[8] X. Yu *et al.*, "Exploring THz band for high speed wireless communications," in *Proc. 41st Int. Conf. Infr., Millim. Terahertz Waves (IRMMW-THz)*, Copenhagen, Denmark, Sep. 2016, pp. 1–2.

[9] E. Lacombe *et al.*, "10-Gb/s indoor THz communications using industrial Si photonics technology," *IEEE Microw. Wireless Compon. Lett.*, vol. 28, no. 4, pp. 362–364, Apr. 2018.

[10] S. Jia *et al.*, "A unified system with integrated generation of high-speed communication and high-resolution sensing signals based on THz photonics," *J. Lightw. Technol.*, vol. 36, no. 19, pp. 4549–4556, Oct.1, 2018.

[11] Z. Wu, M. Liang, W.-R. Ng, M. Gehm, and H. Xin, "Terahertz horn antenna based on hollow-core electromagnetic crystal (EMXT) structure," *IEEE Trans. Antennas Propag.*, vol. 60, no. 12, pp. 5557–5563, Dec. 2012.

[12] J. W. Bowen *et al.*, "Micromachined waveguide antennas for 1.6 THz," *Electron. Lett.*, vol. 42, no. 15, pp. 842–843, Jul. 2006.

[13] B. Andres-Garcia *et al.*, "Gain enhancement by dielectric horns in the terahertz band," *IEEE Trans. Antennas Propag.*, vol. 59, no. 9, pp. 3164–3170, Sep. 2011.

[14] K. Fan, Z.-C. Hao, Q. Yuan, and W. Hong, "Development of a high gain 325–500 GHz antenna using quasi-planar reflectors," *IEEE Trans. Antennas Propag.*, vol. 65, no. 7, pp. 3384–3391, Jul. 2017.

[15] E. Lacombe *et al.*, "Low-cost 3D-printed 240 GHz plastic lens fed by integrated antenna in organic substrate targeting sub-THz high data rate wireless links," in *Proc. IEEE Int. Symp. Antennas Propag. USNC/URSI Nat. Radio Sci. Meeting*, San Diego, CA, USA, Jul. 2017, pp. 5–6.

[16] X. Tu *et al.*, "Diffractive microlens integrated into Nb_5N_6 microbolometers for THz detection," *Opt. Exp.*, vol. 23, no. 11, pp. 13794–13803, Jun. 2015.

[17] H. Wang, X. Dong, M. Yi, F. Xue, Y. Liu, and G. Liu, "Terahertz high-gain offset reflector antennas using SiC and CFRP material," *IEEE Trans. Antennas Propag.*, vol. 65, no. 9, pp. 4443–4451, Sep. 2017.

[18] W. Pan and W. Zeng, "Far-field characteristics of the square grooved-dielectric lens antenna for the terahertz band," *Appl. Opt.*, vol. 55, no. 26, pp. 7330–7336, Sep. 2016.

[19] H.-T. Zhu, Q. Xue, J.-N. Hui, and S. W. Pang, "A 750–1000 GHz *H*-plane dielectric horn based on silicon technology," *IEEE Trans. Antennas Propag.*, vol. 64, no. 12, pp. 5074–5083, Dec. 2016.

[20] Z.-C. Hao, J. Wang, Q. Yuan, and W. Hong, "Development of a low-cost THz metallic lens antenna," *IEEE Antennas Wireless Propag. Lett.*, vol. 16, pp. 1751–1754, 2017.

[21] T. Tajima, H.-J. Song, K. Ajito, M. Yaita, and N. Kukutsu, "300-GHz step-profiled corrugated horn antennas integrated in LTCC," *IEEE Trans. Antennas Propag.*, vol. 62, no. 11, pp. 5437–5444, Nov. 2014.

[22] Y. Liu *et al.*, "Millimeterwave and terahertz waveguide-fed circularly polarized antipodal curvedly tapered slot antennas," *IEEE Trans. Antennas Propag.*, vol. 64, no. 5, pp. 1607–1614, May 2016.

[23] H. Lu, X. Lv, and Y. Liu, "Radiation characteristics of terahertz waveguide-fed circularly polarised antipodal exponentially tapered slot antenna," *Electron. Lett.*, vol. 50, no. 16, pp. 1122–1123, Jul. 2014.

[24] K. Konstantinidis *et al.*, "Low-THz dielectric lens antenna with integrated waveguide feed," *IEEE Trans. THz Sci. Technol.*, vol. 7, no. 5, pp. 572–581, Sep. 2017.

[25] J. Ala-Laurinaho *et al.*, "2-D beam-steerable integrated lens antenna system for 5G *E*-band access and backhaul," *IEEE Trans. Microw. Theory Techn.*, vol. 64, no. 7, pp. 2244–2255, Jul. 2016.

[26] O. Yurduseven, N. L. Juan, and A. Neto, "A dual-polarized leaky lens antenna for wideband focal plane arrays," *IEEE Trans. Antennas Propag.*, vol. 64, no. 8, pp. 3330–3337, Aug. 2016.

[27] N. Llombart *et al.*, "Silicon micromachined lens antenna for THz integrated heterodyne arrays," *IEEE Trans. THz Sci. Technol.*, vol. 3, no. 5, pp. 515–523, Sep. 2013.

[28] K. Guo, A. Standaert, and P. Reynaert, "A 525–556-GHz radiating source with a dielectric lens antenna in 28-nm CMOS," *IEEE Trans. THz Sci. Technol.*, vol. 8, no. 3, pp. 340–349, May 2018.

[29] P. Nayeri *et al.*, "3D printed dielectric reflectarrays: Low-cost high-gain antennas at sub-millimeter waves," *IEEE Trans. Antennas Propag.*, vol. 62, no. 4, pp. 2000–2008, Apr. 2014.

[30] H. Yi, S.-W. Qu, K.-B. Ng, C. H. Chan, and X. Bai, "3-D printed millimeter-wave and terahertz lenses with fixed and frequency scanned beam," *IEEE Trans. Antennas Propag.*, vol. 64, no. 2, pp. 442–449, Feb. 2016.

[31] B. Zhang *et al.*, "Metallic 3-D printed antennas for millimeter- and submillimeter wave applications," *IEEE Trans. THz Sci. Technol.*, vol. 6, no. 4, pp. 592–600, Jul. 2016.

[32] W. J. Otter *et al.*, "3D printed 1.1 THz waveguides," *Electron. Lett.*, vol. 53, no. 7, pp. 471–473, 2017.

[33] B. Zhang and H. Zirath, "Metallic 3-D printed rectangular waveguides for millimeter-wave applications," *IEEE Trans. Compon., Packag., Manuf. Technol.*, vol. 6, no. 5, pp. 796–804, May 2016.

[34] J. Li, T. Ma, K. Nallapan, H. Guerboukha, and M. Skorobogatiy, "3D printed hollow core terahertz Bragg waveguides with defect layers for surface sensing applications," in *Proc. 42nd Int. Conf. Infr., Millim. Terahertz Waves (IRMMW-THz)*, Cancun, Mexico, Aug./Sep. 2017, p. 1.

[35] F. Wang and T. Arslan, "Microfluidic frequency tunable three-dimensional printed antenna," in *Proc. IEEE MTT-S Int. Microw. Symp. Dig.* , Pavia, Italy, Sep. 2017, pp. 1–3.

[36] MONOCURE Advanced 3D Printer Resins. (Jul. 2018). *MONOCURE 3DR3582C 3D RAPID UV Resin—Clear*. [Online]. Available: http://monocure3d.com.au/v/vspfiles/DATASHEETS/3DR3582C.pdf

[37] Keysight Technologies. (Jun. 2005). *Free Space Materials Measurement Seminar*. [Online]. Available: https://www.keysight.com/upload/cmc_upload/All/FreeSpaceSeminarRev2.pdf

[38] ANYCUBIC. (Dec. 2017). *ANYCUBIC Photon User Manual_English_20171229*. [Online]. Available: http://www.anycubic3d.com/support/show/594032.html

NONCHANUTT CHUDPOOTI (S'16–M'18) received the B.Sc. degree (Hons.) in industrial physics and medical instrumentation and the Ph.D. degree in electrical engineering from the King Mongkut's University of Technology North Bangkok, in 2012 and 2018, respectively, where he was appointed as a Lecturer at the Department of Industrial Physics and Medical Instrumentation, Faculty of Applied Science, in 2018. His main research interests include the application of microwave microfluidic sensors, millimeter-wave substrate integrated circuit applications, and substrate integrated waveguide applications. He was a recipient of the Best Presentation Award from the Thailand-Japan Microwave, in 2015 and 2018, and the Young Researcher Encouragement Award, in 2016.

NATTAPONG DUANGRIT was born in Chiangmai, Thailand, in 1991. He received the B.Eng. degree from the Rajamangala University of Technology Thanyaburi, in 2014. He is currently pursuing the Ph.D. degree with the King Mongkut's University of Technology North Bangkok. His Ph.D. was supported by the Thailand Research Fund through the Royal Golden Jubilee Ph.D. Program.

His main research interests include the application of 3D printing technology for millimeter-wave and THz devices and substrate integrated waveguide applications.

PRAYOOT AKKARAEKTHALIN (M'98) received the B.Eng. and M.Eng. degrees in electrical engineering from the King Mongkut's University of Technology North Bangkok (KMUTNB), Bangkok, Thailand, in 1986 and 1990, respectively, and the Ph.D. degree from the University of Delaware, Newark, DE, USA, in 1998. From 1986 to 1988, he was a Research and Development Engineer with Microtek Products Co., Ltd., Thailand. In 1988, he joined the Department of Electrical Engineering, KMUTNB. He was the Head of the Senior Research Scholar Project which is supported by the Thailand Research Fund, from 2015 to 2017. He has authored or co-authored more than 40 international journals, more than 200 conference papers, and four books/book chapters. His current research interests include RF/microwave circuits, wideband and multiband antennas, telecommunication, and sensor systems. He is a member of IEICE, Japan, ECTI, and the EEAAT Association, Thailand. He was the Chairman of the IEEE MTT/AP/ED Thailand Joint Chapter, from 2007 to 2010, and the Vice President and the President of the ECTI Association, Thailand, from 2012 to 2013 and from 2014 to 2015, respectively. He was the Editor-in-Chief of the ECTI Transactions, from 2011 to 2013.

IAN D. ROBERTSON (F'12) received the B.Sc. (Eng.) and Ph.D. degrees from King's College London, London, U.K., in 1984 and 1990, respectively. From 1984 to 1986, he was with the GaAs MMIC Research Group, Plessey Research, Caswell, U.K. Then, he returned to King's College, initially as a Research Assistant working on the T-SAT project and, then, as a Lecturer leading the MMIC Research Team, where he became a Reader, in 1994. In 1998, he became a Professor of microwave subsystems engineering with the University of Surrey, where he established the Microwave Systems Research Group and was a Founding Member of the Advanced Technology Institute. In 2004, he was appointed to the Centenary Chair in Microwave and Millimetre-Wave Circuits, University of Leeds. He was the Director of learning and teaching, from 2006 to 2011, and the Head of the school, from 2011 to 2016.

Dr. Robertson was the General Technical Programme Committee Chair of the European Microwave Week, in 2011 and 2016.

NUTAPONG SOMJIT (M'10) received the Dipl.-Ing. (M.Sc.) degree from the Dresden University of Technology, in 2005, and the Ph.D. degree from the KTH Royal Institute of Technology, in 2012. Then, he returned to the Dresden University of Technology to lead a research team in micro-sensors and MEMS ICs for the Chair for Circuit Design and Network Theory. In 2013, he was appointed as a Lecturer (Assistant Professor) at the School of Electronic and Electrical Engineering, University of Leeds. His main research interests include integrated smart high-frequency components, heterogeneous integration, and low-cost microfabrication processes.

Dr. Somjit has been a member of the International Editorial Board of the *International Journal of Applied Science and Technology*, since 2013. He was appointed as a member of the Engineering, Physical and Space Science Research Panel of the British Council, in 2014. He was a recipient of the Best Paper Award (EuMIC prize) from the European Microwave Week, in 2009. He received a Graduate Fellowship from the IEEE Microwave Theory and Techniques Society, in 2010 and 2011, and the IEEE Doctoral Research Award from the IEEE Antennas and Propagation Society, in 2012. In 2016, he was the Chair of the Student Design Competition for the European Microwave Week. In 2018, he was appointed as an Associate Editor of IET *Electronics Letters*.